CHAPTER 2

BACKGROUND AND LITERATURE REVIEW

There are many perovskite-type compounds with various properties. There are insulators, dielectrics, magnetic materials, ionic conductors, mixed conductors, and superconductors. Some are chemically quite active and good catalysts while others are inactive. This study is focusing on the use of mixed conducting perovskites as membranes in catalytic reactors for the methane partial oxidation reaction. The background literature survey includes the general review of perovskite-type structure and related ionic and electronic conductivity, phase transformations of perovskites in a reducing atmosphere, perovskite synthesis methods, and the oxygen permeation through a perovskite membrane.

2.1 Structure of Perovskites

2.1.1 Crystal Structure

The ideal perovskite-type oxide structure is cubic with the generic formula ABO_3, where A is the larger cation in a twelve-fold coordination and B is the smaller cation in a sixfold coordination with oxygen ions. Perovskite also can be regarded as a framework structure (ReO_3–type framework), constructed from coner-sharing (BO_6) octahedral with A ions placed in twelve-coordinate interstices (Figure 2.1a). Alternatively, the structure can be viewed with the B cation in the center, as shown in Figure 2.1b. Each oxygen ion is coordinated with two B ions and four A ions. It was pointed out that the most important prerequisite for a stable perovskite structure is the existence of a stable BO_3 skeletal sublattice [19]. From geometric considerations, the B cation radius must exceed 0.051 nm to achieve stable octahedral coordination in oxide based perovskites. The BO_3 skeletal sublattice can be further stabilized by the large A site cations in cubo-octahedral coordination at the center of eight BO_6 octahedrons. The presence of the A-site cation generally distorts the BO_3 Skeletal sublattice in order to attain optimal A-O bond lengths where the lower limits for

cationic radii are $r_A > 0.09$ nm. When this distortion is too large, other crystal geometries such as orthorhombic or rhombohedral become favorable.

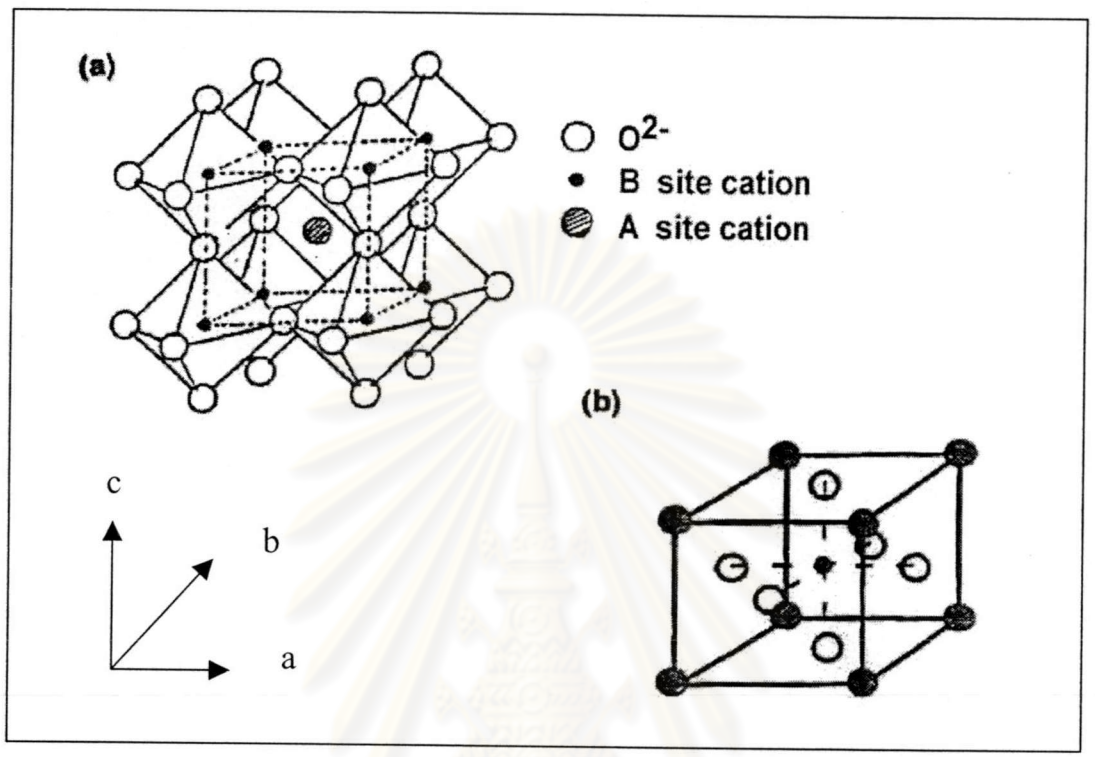

Figure 2.1 (a) Corner-sharing (BO_6) octahedral and with A ions placed in twelve-coordinate interstices,
(b) Cation B at the center of the unit cell [20]

In the ideal structure, where the atoms are touching one another, the B-O distance is equal to a/2 (a is the cubic unit cell parameter) while the A-O distance is (a/2) and the following relationship between the ionic radii holds: $r_A + r_O = \sqrt{2}\,(r_B + r_O)$. However, it was found that the cubic structure was still retained the ABO_3 compounds, even though this equation is not exactly obeyed. As a measure of the deviation from the ideal structure, Goldschmidt [21] defined the tolerance limits of the size of ions through a tolerance factor, t as Equation (1)

$$\text{when} \qquad t = (r_A + r_O)/\,[\sqrt{2}\,(r_B + r_O)] \qquad (1)$$

where r_A, r_B, and r_O are the radii of respective ions. t would be equal to one for the ideal structure. In fact, the perovskite structure exists in oxides only between the

limits $0.75 < t < 1.0$ with t between 0.8 and 0.9 in most cases. For tolerance factors between limits $0.9 < t < 0.75$, a cooperative buckling of the corner shared octahedron takes place, leading to orthorhombic distortion. When there is octahedral buckling, a small deformation from cubic to rhombohedral symmetry may take place. This occurs for tolerance factors between $0.9 < t < 1.0$ [20].

Besides the ionic radius requirements, the other requirement to be fulfilled is electroneutrality, i.e., that the sum of charges of A and B ions equals the total charge of O anions. It is attained in the case of oxides by means of charge distribution of the form $A^{1+}B^{5+}O_3$, $A^{2+}B^{4+}O_3$, or $A^{3+}B^{3+}O_3$. The survey of the chemical elements that are known to be stable in the A, B, and or X positions of the perovskite structure was reported by Goodenough et al [20]. The data on the structure and properties of this type of compound show that almost all the stable elements have been included in the perovskite framework, many of them were in both the A and B positions.

2.1.2 Nonstoichiometry in Perovskites

Nonstoichiometry in perovskites can arise from either cation deficiency (in the A or B site), anion deficiency, or anion excess. However, the partial substitution of A and B ions giving rise to complex oxides has to keep the perovskite structure. For the cation deficiency, A-Site cations can be missing without collapse of the perovskite network because of the stability of the BO_3 group [22]. On the contrary, B-site vacancies are not energetically favored because of the large formal charge and the small size of the B cations in perovskites [19]. Nevertheless, an oxygen vacancy in perovskites is more common than a cation deficiency.

Many oxygen-deficient perovskites can be described on the basis of complex perovskite-related super-structures of general formula $A_nB_nO_{3n-1}$, in which the stacking manner depends on the size, electronic configurations, and coordination numbers of A and B cations. Oxygen vacancies are accomplished by substituting ions of similar size but different valence. For example, some of the La^{3+} ions in $LaBO_3$ are replaced by Sr^{2+} to form $La_{1-x}Sr_xBO_{3-\delta}$, and, therefore, oxygen vacancies are formed. The former composition can be considered as an anion-deficient perovskite with one-sixth of the oxygen ions being vacant. Oxygen vacancies are ordered in alternate [001] BO_2 planes of the cubic structure such that alternate [110] rows of oxide anions are missing.

2.1.3 Physical Properties

In characterization of materials, it is more often to measure their electronic and ionic conductivity than concentrations of electrons (holes) and mobile ions (vacancy). The calculated ionic and electronic conductivity were separately measured by using 4-probe ionic d.c. and ordinary 4-probe d.c. techniques, respectively.

For all materials that are in principle nonzero electronic and ionic conductivity, the overall electrical conductivity σ_{tot} is the sum of electronic conductivity σ_e and ionic conductivity σ_i, as Equation (2),

$$\sigma_{tot} = \sum \sigma_{ij} + \sigma_e \qquad (2)$$

where σ_{ij} is the partial conductivity (in $\Omega^{-1}cm^{-1}$) of the *jth*-type ionic charge carriers presenting in the solid. Ionic charge carriers can be either atomic in nature or normally defects of either the anionic or cationic sublattice. Ionic conductivity occurs normally via interstitial sites or by hopping into a vacant site (vacancy motion) or a more complex combination based on interstitial and vacant sites.

Electronic (electron/hole) conductivity occurs via delocalized states in the conduction-valence band or via localized states by a thermally assisted hopping mechanism. The presence of electronic conduction in perovskites proceeds via B

$$B^{n+} - O^{2-} - B^{(n+1)+} \longrightarrow B^{(n+1)+} - O^{2-} - B^{(n+1)+} \longrightarrow B^{(n+1)+} - O^{2-} - B^{n+} \qquad (3)$$

lattice cations through overlapping B-O-B bonds via a mechanism known as the Zerner double exchange process as shown in Equation (3) [20]:

This process is facilitated by strong overlap of the B site cation and O^{2-} orbital which is maximized for B-O-B angles at 180°C, i.e., cubic structure. In the orthorhombic structure, the tilting of BO_6 octahedron gives rise to a decrease in the B-O-B overlap and thus would be expected to provide a larger barrier to electronic conduction. In the above double exchange mechanism, electronic conduction requires the presence of B site cations with multiple valences. Furthermore, the electronic conduction can be n-type or p-type, depending on the material properties and ambient oxygen partial pressure. The energy level shifts from the center of the energy gap toward the empty zone for an n-type semiconductor or the filled band for a p-type semiconductor [23]. An n-type conductor is an electron conductor while a p-type

conductor is an electron hole conductor. It was noticed that perovskites with high p-type electronic conductivity tended to be active for deep methane oxidation reactions while those with high n-type electronic conductivity, ionic conductors, and insulators were all found to be more selective to C_2 compounds [24].

Electronic conductivity in perovskites can arise from thermal excitation of electrons from the valence band, which is oxygen 2p orbital, to the conduction band, which is t_{2g} orbital of the B-site cation [20]. Also, at elevated temperatures, the energy barrier is low enough that oxygen ions can diffuse through the structure from vacancy to vacancy. Two types of adsorbed oxygen, α- and β-species, were observed in the temperature desorption curves of oxygen from $La_{1-x}Sr_xCoO_{3-\delta}$ [25]. Detailed investigation revealed that α-oxygen desorbed below 800°C was adsorbed on oxygen vacancies that were created by the substitution of Sr^{2+} for La^{3+}, whereas desorption of β-oxygen accompanied the partial reduction of Co^{3+} to Co^{2+}.

Mixed ionic-electronic conductors exhibit both ionic and electronic conductivity, for example $La_{1-x}Sr_xBO_{3-\delta}$. When the B ions can take a mixed-valence state, charge neutrality is maintained by both the formation of oxygen vacancies and a change in the valence state of the B ions. The oxides may show both a high oxygen ion conductivity due to the high oxygen vacancy concentration, and a high electronic conductivity due to the mixed-valence state [26]. The concentration of oxygen vacancies can also be increased by a mild B-site ion substitution, such as Cu and Ni ions which naturally take the divalent oxidation state [27]. If the valence state of the B ions is fixed, neutrality is maintained only by the formation of oxygen vacancies. The oxides may be predominantly ionic conductors in this case.

The dependence of the electrical conductivity as a function of doping is reported by many researchers. For examples, the electrical conductivity of $La_{1-x}Sr_xGa_{1-y}Mg_yO_{3-\delta}$, LSGM, at 613-1,023°C as a function of doping with equal quantities of Sr and Mg (x = y) was studied by Gorelov et al [28]. When $LaGaO_3$ was doped with equal amounts of Sr and Mg at the step x = y = 0.05, electrical conductivity of LSGM increased with doping, up to its maximum value at x = y = 0.15. The next composition with x = y = 0.20 had much lower conductivity and the sample was not monophasic. The $LaSrGa_3O_7$ and $La_4Ga_2O_9$ phases were present in large quantities. Thus, the maximum electrical conductivity of this system corresponds to the region of saturation limits of Sr and Mg in LSGM.

The p-type electronic conductivity of $La_{0.9}Sr_{0.1}Ga_{1-x}Me_xO_{3-\delta}$ (Me = Fe or Cr and x = 0, 0.05, or 0.20) materials was confirmed to be strongly influenced by the content of Fe because the formation of Fe^{3+}/Fe^{4+} was easier than that of Cr^{3+}/Cr^{4+}. The conductivity increased and activation energy of conduction decreased with increasing degree of substitution. The activation energy for p-type conductivity was found to be in the range 0.9-1 eV, lower than usually observed for alternative electrolytes based on zirconia or ceria. [12]

Partial substitution of Ga in $La_{0.9}Sr_{0.1}(Ga_{1-y}M_y)_{0.8}Mg_{0.2}O_{3-x+\delta}$, LSGM, by the transition metals M = Cr, Mn, Fe, Co seems to be an efficient method to modify the electrical properties of LSGM. For $y > 0.1$ $\log\sigma_{tot}$ increases proportionally to the dopant content caused by increasing the p-conductivity. When doped with the amount $y \leq 0.1$ of Fe or Co, the electrical conductivity is nearly independent of y and gallates exhibit oxygen ionic conductivity more than twice that of LSGM [29].

Temperatures also play an important role in ionic and electronic conductivity. This can be expressed by the Arrheius equation in Equation (4):

$$\sigma = A \exp\left(-\frac{Ea}{RT}\right) \tag{4}$$

where Ea is the activation energy, R is the universal gas constant, and T is the absolute temperature (in K). The pre-exponential factor, A, contains several constants, including the vibrational frequency of the potentially mobile ions, and depend on the structure of materials and type of charge carriers.

2.2 Dense Perovskite Membranes for Oxygen Separation

Dense perovskite membranes exhibiting high oxygen ionic and electronic conductivity have become of great interest as a potentially economical, clean and efficient means of producing oxygen by separation from air or their oxygen containing gas mixtures. However, these processes required the sufficiently high temperatures, typically above about 700°C.

In this section, a brief overview is given of major membrane concepts, and oxygen permeation through a mixed-conducting membrane.

2.2.1 Major Membrane Concepts

The separation of oxygen using an mixed ionic-electronic conducting (MIEC) membrane is schematically shown in Figure 2.2.

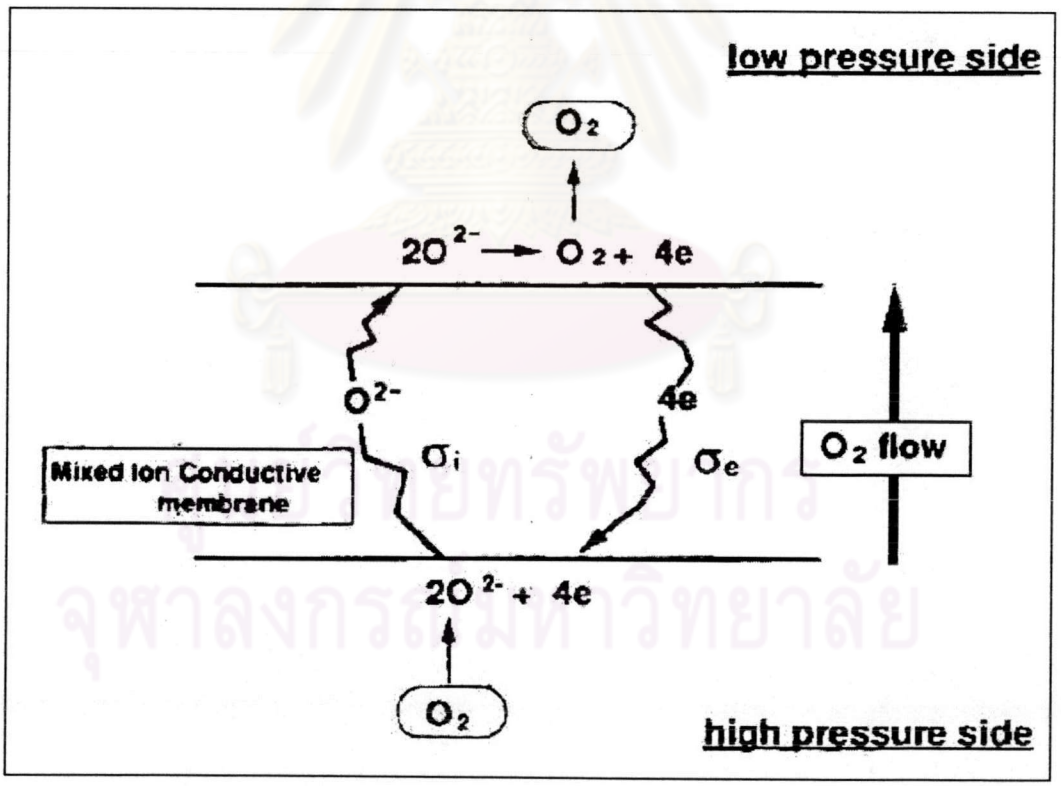

Figure 2.2 Oxygen transport in a mixed ion conductor

The driving force for overall the oxygen transport is the differential oxygen partial pressure applied across the membrane. As the MICE membrane is dense and gas-tight, the direct passage of oxygen molecules is blocked, yet oxygen ions migrate selectively through the membranes. Dissociation and ionization of oxygen occurs at the oxide surface at the high-pressure side (feed side, P'_{O_2}), where electrons are picked up from accessible (near-) surface electronic states. The flux of oxygen ions is charge compensated by a simultaneous flux of electronic charge carriers. Upon arrival at the low pressure side (permeate side, P''_{O_2}), the individual oxygen ions with their electrons recombine again to form oxygen molecules, which are released in the permeate stream.

Normally all oxides transport to some degree mixed ionic and electronic conduction and selective oxygen has been reported even for dense sintered alumina above 500°C [30, 31]. Although it is common to speak of mixed conduction when the total conductivity is provided by near equal fractions of the partial ionic and electronic conductivity, respectively [32], from the point of view of oxygen permeation it is more useful to relate mixed conduction property to their absolute values. The volume diffusion theory for ambipolar transport in oxides clearly indicate that higher currents (fluxes) are obtained when either the electronic or the ionic conductivity increases, or both increase simultaneously. The flux at a given total conductivity is at maximum when the ionic and electronic transference numbers are equal, i.e. 0.5. In this view, alumina is not a good mixed conductor. Materials showing predominant electronic conduction may prove to be excellent mixed conductors when their ionic conductivity is substantial. The general objective for optimum membrane performance therefore is to maximize the product of the mobility and concentration of both ionic and electronic charge carriers in appropriate ranges of temperature and oxygen partial pressure.

Owing to the ability to conduct both oxygen ions and electrons, the MIEC membrane can operate without the need of attachment of electrodes to the oxide surface and external circuitry.

Two routes have been used to enhance the oxygen permeation rate. The first is to fabricate a very thin layer of oxygen ion conducting material on top of a porous support [33, 34]. In the second approach, new materials have been developed with high oxygen permeability, due to the presence of mixed conduction. Mixed

conductors such as some perovskites (generic formula ABO_3) have been reported to have permeation rates one or two orders of magnitude greater than those of stabilized zirconia [35]. The partial substitution of A-site cations by other metal cations with lower valences usually causes the formation of oxygen vacancies and the appearance of ionic conduction. Substitution of a transition metal with variable valence at the B site can lead to high ionic conductivity. Recent reports suggest that there is considerable commercial interest in the use of dense perovskite membrane reactors to carry out the methane partial oxidation to syngas reaction if sufficiently high oxygen-permeation rates can be achieved [27].

Some perovskite materials, however, have very high oxygen permeation abilities but poor stabilities in a reducing atmosphere at elevated temperatures. One of the examples is $SrFe_{0.2}Co_{0.8}O_{3-\delta}$ (SFCO). This perovskite has a high reported oxygen permeation rate, 0.023 $molm^{-2}s^{-1}$ [35] (800°C at pressure gradient of 1 atm, but has a sudden phase transformation at around 790°C [36] and reducing atmosphere [37]. The $Sr(Co, Fe)O_{3-\delta}$ membrane of Pei et al. [37] cracked due to the high oxygen partial pressure gradient across the membrane, right after the syngas reaction was turned on, indicating that the lattice structure was depended on the oxygen partial pressure. The membrane was also reduced to $SrCO_3$ and elemental Co and Fe after a couple of days, indicating that either the mismatch of the perovskite lattice parameters or the decomposed products caused considerable volume expansion leading to the fracture [37]. Takeda et al. [38] also pointed out that the crystal structure of $SrCoO_3$ powder was apt to be changed by temperature, ambient oxygen partial pressure, and synthetic conditions. Therefore, a compromise between high permeability and stability for perovskite membrane materials is necessary.

2.2.2 Oxygen Permeation through a Mixed-Conducting Membrane

The mechanism of oxygen permeation through a mixed-conducting membrane can be described as follows [39]:

1. Oxygen transport from the gas phase with high oxygen partial pressure to the membrane surface.
2. Physical adsorption on the surface.

3. Dissociation and electron transfer, giving chemisorbed oxygen species.
4. Incorporation in membrane surface layer.
5. Diffusion of lattice defects to interior.
6. Removal from the opposite membrane surface layer.
7. Association and electron transfer, forming chemisorbed oxygen species.
8. Desorbtion from the surface
9. Transport from the membrane surface to the gas phase with low oxygen partial pressure.

From a macroscopic view, the membrane may be divided into three regions: a central bulk zone and adjacent zones, emphasizing the importance of both solid-state diffusion and surface exchange reactions to the extent of oxygen permeation (Figure 2.3). The mechanism for oxygen transport through the membrane can be bulk diffusion control, surface control, or a mixed type of rate control [40].

For the predominant of bulk diffusion, the oxygen flux can be increased by reducing the thickness of the membrane, until its thickness becomes less than a characteristic value, L_c, at which point the flux of oxygen is under conditions of mixed control of the surface exchange kinetics and bulk diffusion [41]. Below L_c, the oxygen flux, in the case of the predominant of surface control, can be improved by optimization of the surfaces, e.g. by enhancing the surface area and/or addition of suitable catalytic materials.

Traditionally, the oxygen permeation flux across a MIEC membrane can be calculated using the Wagner equation, which assumes the oxygen bulk diffusion along the thickness L to be the rate-limiting step. [42]

$$J_{O_2} = \frac{RT}{16F^2L}\int_{\ln P''_{O_2}}^{\ln P'_{O_2}} \frac{\sigma_e\sigma_i}{\sigma_e + \sigma_i}\, d\ln P_{O_2} \qquad (5)$$

where F is Faraday's constant, R the gas constant, T the temperature and σ_e and σ_i signify electronic and ionic conductivity, respectively. P'_{O_2} and P''_{O_2} are the equivalent oxygen partial pressures in the outer most layers of the membrane on the feed side and the permeate side of the membrane, respectively. The limit of integration is the oxygen partial pressures maintained at the gas phase boundaries.

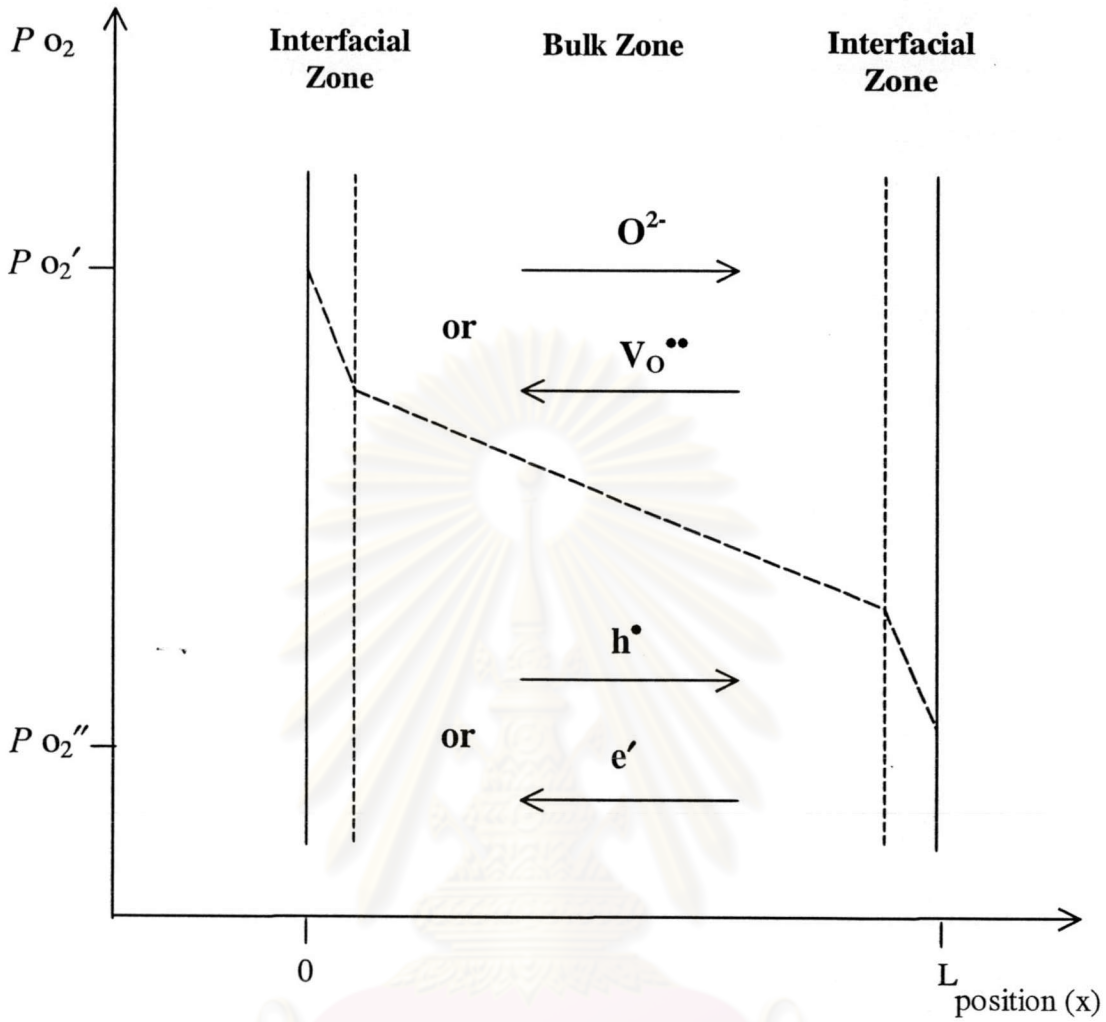

Figure 2.3 Illustration of the principle in a MICE membrane at various zones during steady state oxygen permeation. The curve shows a possible P_{O_2} profile over the membrane. A single prime indicates air side, double prime indicates permeate side.

Equation (5) may be evaluated numerically from experimental data on the P_{O_2} dependence of the ionic and electronic conductivity. However, to carry out the further derivation, the defect chemistry of a specific material system has to be considered.

The Equation (5) can be integrated in the simplest way upon the concept that oxygen ions and electrons diffuse in a way shown in Figure 2.3 [7]. The total current density, j_{tot} ($= j_e + j_{O2-}$), which is the sum of the electronic and ionic partial current,

can be regarded to be zero under steady state. Therefore, the actual oxygen flux expressed in terms of volume unit, Jo_2 [cm^3 (STP)/cm^2 min], can be given as follows,

$$Jo_2 = j_{O2-} / 4F$$

$$= \frac{RT \quad \sigma_e \sigma_i}{16 F^2 (\sigma_e + \sigma_i) L} \ln\left(\frac{P'o_2}{P''o_2}\right) \qquad (6)$$

When the electronic conductivity is larger than the ionic conductivity, Equation (6) can be approximated by

$$Jo_2 = 7.5*10^{-5} \frac{T\sigma_i}{L} \ln\left(\frac{P'o_2}{P''o_2}\right) \qquad (7)$$

Following Equation (7), the oxygen permeation rate is governed by two factors, thickness of membrane and partial pressure of oxygen in the feed. Itoh et al. [43] reported the oxygen flux increased from 0.15 to 0.3 cm^3 (STP)/cm^2 min when decreasing the $La_{0.4}Sr_{0.6}CoO_3$ membrane thickness from 0.14 to 0.06 cm, respectively, at 1,021 K. In agreement with the bulk diffusion-controlled theory, oxygen permeation rate monotonously increased with decreasing thickness of the $La_{0.7}Sr_{0.3}Ga_{0.6}Fe_{0.4}O_{3-\delta}$, membrane and the oxygen permeating rate at 900°C attained to a value of 2.5 cm^3 (STD)/cm^2.min when the thickness of this membrane was 0.3 mm. Therefore, the rate determining step for oxygen permeation through Sr- and Fe-doped $LaGaO_3$ perovskite membrane seems to be bulk diffusion process and consequently, it is expected higher oxygen permeation rate can be obtained by decreasing the thickness of the membrane.

The results reported by Xu and Thomson [44] and van Hassel et al. [45] indicate that the Wagner equation is not the prediction in the presence of reactions at the surface of those perovskite membranes. Even if there is no surface oxidative reaction, oxygen ion surface exchange kinetics may exert partial or dominant control on oxygen permeation under certain conditions.

Among the surface exchange process, the exchange of oxygen between oxide surfaces and the gas phase has been recognized to involve a series of reaction steps. Each of the steps may be the rate-determining step. Possible steps for the reduction of oxygen include adsorption, dissociation, charge transfer, surface diffusion of

intermediate species (e.g., $O^-_{2\,(ads)}$, $O^-_{(ads)}$, and $O_{(ads)}$), and finally corporation into a boundary layer near the surface. Generally, it is assumed that the reoxidation of oxygen anions follows the same series of steps in the reverse direction. The surface reaction is thus associated with transport of charge.

At lower temperatures, a physical form of oxygen desorption predominates. As the temperature increases, the chemisorption of the dissociation of oxygen molecules and electron transfer become increased, resulting in the formation of various chemisorbed species. Therefore, it is important to be able to modify and/or expand the Wagner theory to account for oxygen permeation with considerations of both bulk diffusion and surface reactions.

The ratio $h = k/D^*$ [46], where k is the surface exchange coefficient and D^*, the tracer diffusion coefficient, has been considered a convenient parameter in determining the extent to which surface exchange controls the oxygen permeation kinetics. The smaller the h value, the more the surface exchange contributes to the total oxygen permeation resistance relative to bulk diffusion. Similarly, Bouwmesster et al [41] proposed to use a characteristic length (L_c), which is equal to the reciprocal of the ratio h, to describe the possible involvement of surface exchange in limiting the rate of oxygen permeation. The characteristic length can be obtained as the form in Equation (8)

$$L_c = \frac{Ds}{k_s} = \frac{D^*}{k_s} \qquad (8)$$

where D_s is the self-diffusion coefficient of oxygen anions with valence charge –2, D* is the tracer diffusion coefficient, and equal to the self-diffusion coefficient D_s. The characteristic thickness L_c is not the intrinsic property of a membrane and depends on oxygen partial pressure and temperature. Because of the assumption made during its derivation, L_c valid only to cases of small oxygen pressure gradients across the membrane. These parameters require special techniques such as ^{18}O-^{16}O isotopic exchange or secondary in mass spectroscopy (SIMS) in order to determine the surface exchange coefficients. Examples can be found in numerous literature [46,47].

Other efforts have been attempted to correlate the oxygen permeation rate to directly measurable variables such as the oxygen partial pressures at the both sides of

the membrane and the membrane thickness (L) [48]. However, the resulting permeation equations are still too complex to be used for distinguishing between surface exchanges and bulk diffusion. Thus there is high motivation to simplify the oxygen permeation models over ion conducting membranes and to base the analysis on the individual step of the permeation mechanism.

According to the recent study by Pederson et al. [50], the electronic conductivity (σ_e) of $La_{1-x}Sr_xCo_{1-y}Fe_yO_{3-\delta}$ (LSCF) is dramatically higher than its ionic conductivity (σ_i). The ratio of σ_e/σ_i range from 194 for $La_{0.2}Sr_{0.8}Co_{0.2}Fe_{0.8}O_{3-\delta}$ to 1096 for $La_{0.6}Sr_{0.4}Co_{0.2}Fe_{0.8}O_{3-\delta}$. This indicates that the transport of oxygen ions rather than that of electrons overwhelmingly limits the oxygen permeation over an open circuit LSCF membrane.

An explicit oxygen permeation model for ion-conducting perovskite membranes, $La_{0.6}Sr_{0.4}Co_{0.2}Fe_{0.8}O_{3-\delta}$ has been developed to directly correlate the oxygen flux to the readily measurable variables such as temperature, membrane thickness, and the oxygen pressure gradient. In order to determine model parameters such as the oxygen vacancy bulk diffusion coefficient and the surface exchange rate constants, measurements of oxygen fluxes were conducted on a 3.99-mm thick disk by independently changing temperature and oxygen partial pressures at both sides of the membrane. The results of this model indicate that bulk diffusion has an activation energy of 73.6 kJ/mol which is lower than the activation energies for surface exchange kinetics by a factor of about three. Based on permeation analysis, it has been determined that the permeation exerted by surface exchange at the oxygen-rich side is relatively small and negligible under all conditions, which agrees with the experimental observation that with constant T and P''_{O2} , changes in P'_{O2} do not significantly influence the oxygen permeation. Therefore, for most cases, the oxygen permeation is jointly controlled by the surface exchange at the oxygen-lean side and the bulk diffusion. Moreover, it can be concluded that at low temperatures (around 760^0C), the oxygen permeation is rate-limited by the surface exchange at the oxygen-lean side, while it is dominantly controlled by bulk diffusion at high temperatures (around 950^0C). The effect of P''_{O2} has also been predicted with the model and it is demonstrated that as long as $P''_{O2} << P'_{O2}$ changes in P''_{O2} only influence the bulk diffusion [44].

Besides the bulk diffusion and surface exchange, the effect of sweep gas flow rate and the effect of microstructure, including grain boundary diffusion, may also influence the overall oxygen transport. Itoh et al (1994) showed the effect of the sweep gas flow rate on the oxygen flux across the $La_{0.6}Sr_{0.4}CoO_{3-\delta}$ disk. It was found that the permeation rate is almost constant when the sweep gas flow rate is greater than 50 cm^3/min, where the so-called mass transfer resistance to oxygen between the membrane surface and the bulk gas is regarded to be negligibly small compared to that of the oxygen transport across the membrane [43].

Zhang et al. [50] reported the effects of microstructure on the oxygen permeation in $SrCo_{0.8}Fe_{0.2}O_{3-\delta}$ (SCFO) and $La_{0.2}Sr_{0.8}Fe_{0.8}Cr_{0.2}O_{3-\delta}$ (LSFCO) by using disk samples fabricated under different processing conditions. The microstructure of LSCF2828 remained unchanged when the sintering temperature was increased from 1,300 to 1,450°C, but the average grain size of SCF1082 increased considerably when the sintering temperature was increased from 930 to 1200°C. The change in the grain size was found to have a strong effect on the oxygen permeation flux in SCF1082, which increased considerably as the grain size was decreased. This indicated that the contribution of the grain boundary diffusion to the steady state oxygen flux in SCF1082 was substantial and grain boundaries provided faster diffusion paths in oxygen permeation through the sample.

2.3 Perovskite Containing Different Metals

The ideal features of ABO_3-based perovskites for preparing the membranes for the oxygen permeation are then concluded to be as follows; having a high oxygen permeability, being stable under a harsh chemical environment, and having a stable lattice structure under changes in oxygen partial pressure. It has been reported that all compounds below have the above properties.

2.3.1 Cobalt-Containing Perovskite

Powder compositions in the series $La_{1-x}A_xCo_{1-y}Fe_yO_{3-\delta}$ (A = Sr, Ca) exhibited high electrical conductivity with appreciable oxygen-ion conductivity that increased with Co content for the compositions studied. Oxygen permeation studies showed a significant flux of oxygen that increased with temperature for specimens in a $P(O_2)$ gradient with no applied field. Thermogravimetric studies of the $La_{1-x}A_xCo_{1-y}Fe_yO_{3-\delta}$ system indicated a mass loss that increased with temperature [50]. This weight loss, which tended to increase with increasing Sr content, was observed at elevated temperatures as the materials became increasingly oxygen deficient (vacancy). This caused the membrane to have the high oxygen permeation rate at high temperature.

2.3.2 Barium-Containing Perovskite

For comparison, the structure of $SrCo_{0.8}Fe_{0.2}O_{3-\delta}$ at 800°C changed from cubic perovskite to brownmillerite-type structure when the oxygen partial pressure was lower than 0.1 atm. The oxygen flux of the $Ba_{0.5}Sr_{0.5}Co_{0.8}Fe_{0.2}O_{3-\delta}$ membrane was as high as 1.1 $cm^3/cm^2.min$ at 850°C and very stable during the 1,040 hours running time. At 850°C, 90% CH_4 conversion and 98% CO selectivity was obtained. The oxygen permeation flux, under partial oxidation of methane reaction conditions, increased to around 8 $cm^3/cm^2.min$, which was eight times higher than the permeation under air/He oxygen partial pressure gradients. It was also two-fold that of SCF1082 and LBCF2828 membrane under oxidation reaction operation [51].

2.3.3 Lanthanum Gallate Perovskites

Ishihara et al. (1999) compared the ionic conductivity of doped $LnGaO_3$ (Ln=La, Pr, Nd) perovskite type oxide. They found that ionic conductivity increased with increasing the ionic radius of A site cation. Therefore, the gallate ABO_3 with A = La has the highest oxygen ionic conductivity and correspondingly the highest Goldschmidt tolerance factor in relation to other A = rare earth occupations. Investigations on lanthanum compounds with the three-valent cations Al, Ga, In, Sc, Lu on B site show the maximum specific conductivity and oxygen transfer and the minimum of activation energy for Ga. These properties increase with the free volume of the unit cell, on the other hand they decrease with decreasing tolerance factors demonstrating increasing distortion of the perovskite structure. Moreover the advantage of this fast oxide ion conductor is the stability to reduction and oxidation. Therefore, the almost pure oxide ion conductivity is exhibited over a wide range of oxygen partial pressures ($10^{-21} < P_{O2} < 1$ atm) [52].

By doping metal with lower valence but similar size (Ca, Sr, and Ba) on A-site of $LaGaO_3$, oxygen vacancies are generated. Among the dopants, Sr has the optimal effect [53]. The indentation fracture toughness of Sr-substituted gallates was significantly better than the Ca- and Ba-substituted materials [54]. The electrical conductivity increased with an increase in the amount of Sr additives and attained the maximum at x = 0.1 in $La_{1-x}Sr_xGaO_3$. If the Sr content was increased, the secondary phases such as $SrGaO_3$ and La_4SrO_7 were detected by XRD analysis. Therefore, it can be said that the limit of solid solution of Sr exists at about x = 0.1. The formation of secondary phases decreased the oxide ionic conductivity specimens because the electrical conductivity of second phases such as $SrGaO_3$ and La_4SrO_7 was low [9].

The effects of Fe, Co, or Ni doping for Ga site in $LaGaO_3$-based oxide on ionic conductivity was investigated by Ishihara et al. [55]. It was found that the electrical conductivity was greatly improved by these doped metals. The Ni-doped sample gave the highest oxygen permeation rate. A crack formed in the case of $LaCoO_3$-based oxide membrane while there was no crack and no significant change in lattice parameter observed on the Sr- and Fe-doped $LaGaO_3$. Even though doping Ni seems to be the most effective for improving the oxide ion conductivity, with regard to the combination of stability in a reducing atmosphere and oxygen permeation rate, iron is the most suitable dopant for $LaGaO_3$. The oxide ion conductivity was

increased with increasing Fe content. For the study of partial oxidation of methane, it was clear that CH_4 conversion rate was always higher on LSGF8264 than on LSCF6428 used as the oxygen-permeating membrane [10].

Permeation rate of oxygen through Fe doped $LaGaO_3$ membrane (0.5 mm thickness) as a function of x value in $La_{1-x}Sr_xGa_{0.6}Fe_{0.4}O_{3-\delta}$ was studied. Oxygen permeation rate increased with increasing amount of doped Sr and it attained a maximum at x = 0.3. At this composition, the oxygen permeation rate of 1.8 cm^3 (STD)/cm^2.min was achieved at 1,000°C. Therefore, the optimized x value for oxygen permeation in $La_{1-x}Sr_xGa_{0.6}Fe_{0.4}O_{3-\delta}$ exists was at x = 0.3. Since the highest electrical conductivity was also exhibited at x = 0.3, increasing amount of Sr enhanced the amount of oxygen vacancy resulting in the improved oxide ion conductivity in $LaGaO_3$ based oxide. Consequently, the highest oxygen permeating rate was obtained at x = 0.3. It was reported that the oxygen permeation rate of LBCF6482 was 2.1 cm^3 (STD)/cm^2.min at 850°C under similar conditions [56]. Considering the oxygen permeating rate of 1.8 cm^3 (STD)/cm^2.min at 1,000°C, it can be said that LSGF7364 exhibits the high oxygen permeation rate and this material is promising as an oxygen separating membrane from air.

2.4 Perovskite Membrane Synthesis

In order to obtaine the high synthesis of membrane, it is determined to use the combination of raw material powder and processing. This process begins with the synthesis of material with correct compositions, particle sizing, compacting, and sintering.

2.4.1 Wet Chemical Synthesis of Perovskites

It is well known that the synthesis of ceramic powders by using the conventional method or solid state synthesis promotes the crystal growth and resulting in a hard agglomeration. The good sinterability may be achieved when nonagglomerated powders are employed or the preparation procedure is such that weak agglomerates are formed. Therefore, the properties of the raw material powder are important on which several requirements are imposed, fine particles (< 1 μm), narrow size range, no aggregation, controlled particle shape, uniformity in chemical and phase compositions, and high purity [57].

Several techniques, especially wet chemical synthesis or liquid phase synthesis, have been developed from solid-state synthesis to produce the required properties of raw powders, such as precipitation [58], freeze drying [59], spray-pyrolysis, sol-gel [60] and liquid mix process [61], etc.

Liquid mix process is a generic name for various processes that start with a homogeneous solution containing the desired cations, which use additives and evaporation to convert the homogeneous liquid to rigid cross-linked polymer, and which utilize heat to convert the polymer into a homogeneous oxide powder. The initial process was pioneered by Pechini [61] and is referred to either Pechini process. The following steps are used to achieve a powder.

1. An aqueous solution is prepared with metal alkoxides, oxides, hydrated oxides, or carbonates in an alpha-hydroxycarboxylic acid such as citric acid; the ratio of metal ions can be precisely controlled. The acid complexes with the metal ions to form polybasic acid chelates.
2. A polyhydroxy alcohol such as ethylene glycol is added and the liquid is heated to 150 to 250°C to allow the chelates to undergo polyesterification.

3. Heating is continued to remove excess water, resulting in solid polymeric resin.
4. The temperature is increased to about 400°C to char or decompose the resin.
5. The temperature is further increased to 500 to 900°C to form crystallites of the mixed oxide composition. The crystallites are typically 20 to 50 nm and clustered into agglomerates.

Metal oxalates, tartrates, sulphates, nitrates, chlorides, and acetates were avoided because of potentially low solubility of these compounds in either the liquid or the solid resin, which could lead to the phase separation in the final product.

A variety of modifications of the Pechini process have been developed. One was called amorphous citrate process that involves producing precursor from citric acid and metal nitrate before thermal decomposition. For production of Sr-substituted $LaMnO_3$ perovskite powder by the amorphous citrate process, the manganese citrate-nitrate precursor may be represented as in Equation (9)[62]:

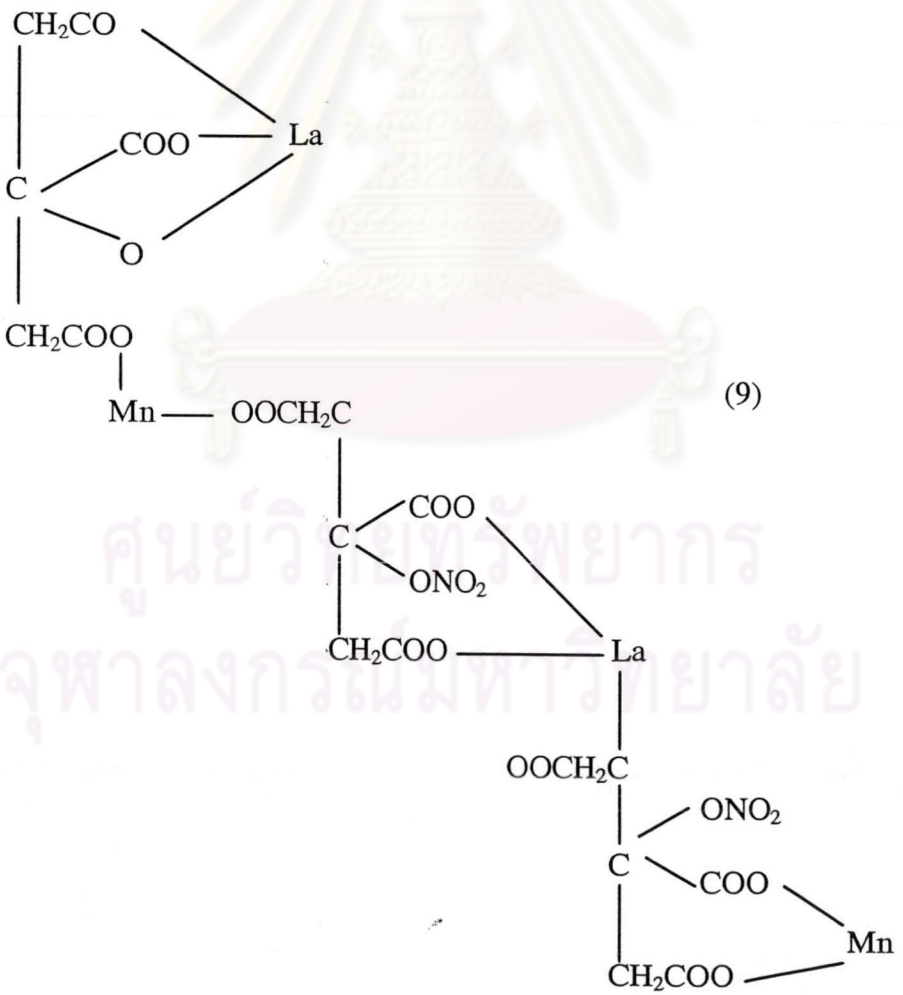

(9)

In the complex the lanthanum is triple charged and replaces in one case the hydrogen of three –COOH groups (as in normal citrate formation) and in another case replaces the hydrogen of one –OH group and two –COOH groups. Manganese in the divalent state replaces the hydrogen in two –COOH groups while NO_2 replaces the hydrogen of one –OH group.

In all cases the minimum amount of citric acid used was that necessary to bond the metals if all the NO_3^- ions were replaced. However, the amounts of metal and citric acid should not be less than equimolar. If the high amount of citric acid was used, Mn_2O_3 was presented as the complex as in Equation (10):

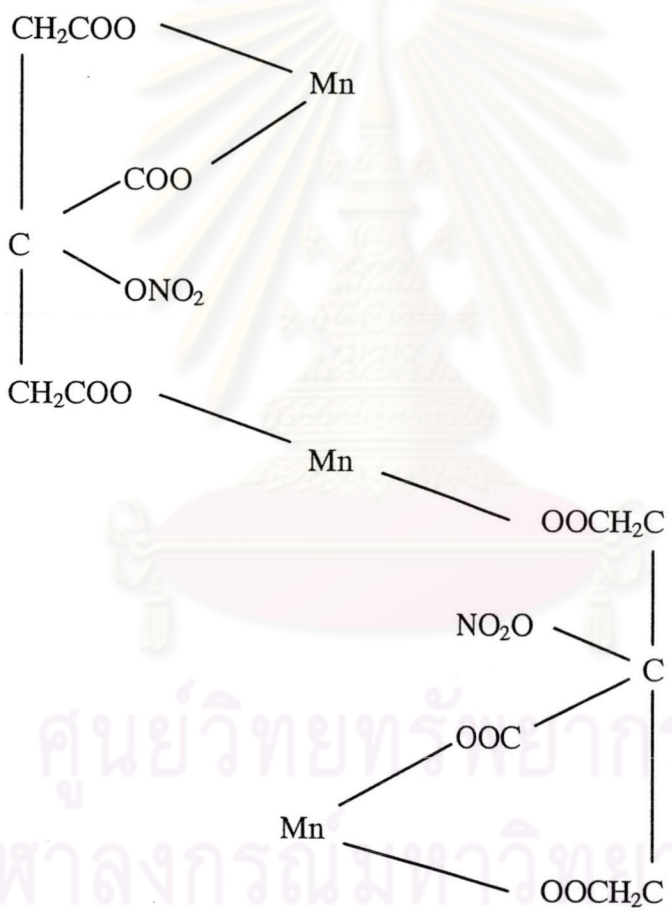

(10)

The formation of the above structure would allow some citric acid, water, and nitrate ions to be lost during the preparation of gel. Every three molecules of citric originally present, one remains uncombined and may be removed from the mixture by either evaporation or decomposition to yield acetone, carbon dioxide and water during the precursor preparation in the vacuum oven. The formation of this complex would also liberate NO_3^- groups for each two molecules of $Mn(NO_3)_2$ originally present in

the solution. The calcination temperature should be higher than 800°C because the wide range of homogeneity at lower temperatures was a result of the segregation of $Sr(NO_3)_2$ during precursor preparation and the production of $SrCO_3$ during precursor decomposition. However it should not be higher than 1,100°C because it would inevitably lead to a decrease in surface area. The best compromise would appear to be the initial treatment of the precursor at 700°C to yield the high surface area followed by an increase in temperature to 1,100°C for a period of up to 4 hours to remove carbon.

Another modifications of the Pechini process were called the citric acid pyrolysis method [63]. For synthesis of $YBa_2Cu_3O_{7-\delta}$, the mixed metal oxides were dissolved by nitric acid. Then the pH value of the dissolved nitrate solution was adjusted by NH_4OH and then NH_4NO_3 served as fuel.

Several synthesis methods have been developed so far. One involves the use of metal nitrates. It is called the glycine-nitrate process, which uses glycine instead of citric acid [64]. The glycine performs two functions. First, it forms complexes with metals cations and increases their solubility. This seems to prevent selective precipitation and segregation during evaporation. Second, the glycine serves as a fuel during charring. Specifically, metal nitrates are combined with glycine in water and evaporated until a homogeneous viscous liquid is formed. The liquid is further heated to about 180°C and auto-ignites. Temperatures rapidly reach 1,100°C to 1,450°C and nearly instantly convert the material to fine, relatively nonagglomerated crystallites of the mixed oxide composition and structure. The glycine nitrate precursor liquid can also be converted to homogeneous mixed oxide powders in a conventional spray drying apparatus.

Teraoka et al. [65] synthesized $La_{0.8}Sr_{0.2}MO_3$ (M = Mn, Co) compounds by a hydroxy acid-aided process which was composed of the evaporation-to-dryness step of the mixed aqueous solution of metal nitrates and a hydroxy acid, followed by calcination in air. When citric or malic acid was used, well-crystallized perovskite-type oxides were formed at 550-600°C, which was 250-300°C lower than the temperature for the conventional nitrate process. The malic acid-aided process gave oxides with larger square surface areas than those obtained with the citric acid-aided process, and the resulting large surface area oxides showed excellent catalytic performance for the combustion of methane.

The malic acid-aided (MAL) process with the adjustment of pH of starting solutions to appropriate values (3.0-3.5 for $La_{0.8}Sr_{0.2}CoO_3$ and 4.0 for $La_{0.8}Sr_{0.2}MnO_3$) was quite effective to produce high surface-area oxides at lower calcination temperatures. The effectiveness of the pH adjustment originated from the formation of homogeneous precursors by the control of the dissociation of carboxylic acid group and the formation of metal-acid complex.

Suresh et al. [66] synthesized $La_{1-x}Sr_xFeO_3$ where x = 0.0-1.0 by the solution combustion method using corresponding metal nitrates, oxalyl dihydrazide (ODH) or tetra formal tris azine (TFTA). Theoretical equation for the formation of ferrite $(LaSr)FeO_3$ assuming complete combustion of the redox mixtures can be written as Equation (11);

$$(1\text{-}x)La(NO_3)_3 + xSr(NO_3)_2 + Fe(NO_3)_3 + 3(CON_2H_3)_2$$

$x = 0\text{-}1.0$

$$\downarrow$$

$$La_{1-x}Sr_xFeO + 6CO_2\,(g) + 9H_2O\,(g) + 9N_2\,(g) \qquad (11)$$

(24 mols of gases /mol of $LaSrFeO_3$)

The powder densities and surface area of TFTA derived ferrites were found to be higher than those of ODH derived ferrites. The average agglomerate size distribution is narrower for ODH derived ferrites than the TFTA ferrites and the average agglomerate sizes are 0.89 μm and 4.8 μm respectively.

The perovskite powders made by wet chemical methods are very fine, and can be nonagglomerated, which facilitates the densification process. The sintering temperature can be several hundred degrees celcius lower for the powders made by wet chemical methods than for those made by conventional solid state synthesis methods. When comparing several techniques in wet chemical methods, liquid mix process is distinguished in the case of less energy consumption, simplest technology, and potential to get fine particles and a single phase powder. Both adding several acids such as citric, malic acid, or etc. and adjusting the pH of aqueous solution are used to provide the fine homogeneous perovskite with the high surface area.

2.4.2 Powder Sizing

Powder particles can influence on compacting and sintering. In most cases the objective of the pressing step is to achieve maximum particle packing and uniformity, so that minimum shrinkage and retained porosity will result during densification. A single particle size does not produce good packing. Optimum packing for particles all the same size results in over 30% void space. Adding particles of a size equivalent to the largest voids reduces the void pore volume to 23%. Therefore, to achieve maximum particle packing, a range of particle sizes is required.

Hard and dense agglomerates in ceramic powders usually result in large interagglomerate pores after sintering [67]. Therefore small particle size is important because it facilitates the high strength of green disc and the sintering process. The primary driving force for densification of a compacted powder at high temperature is the change in surface free energy. Very small particles have high surface areas. The high surface free energy and very strong thermodynamic drive force decrease their surface by bonding them together. The particle with approximate sizes of 1 μm or less can be compacted into a porous shape and sintered at a high temperature to near-theoretical density [68]. Typically, the finer the powder, the greater its surface area, and the lower the temperature and shorter time for densification. Long times at the sintering temperature result in increased grain growth which causes lower strength.

Calcined powder is not usually available with the optimum particle size distribution. The ball milling and screening are the common techniques to achieve the desire particle size of powder.

2.4.3 Powder Compacting by Uniaxial Pressing [68, 69]

Uniaxial pressing is accomplished by placing the powder into a rigid die and applying pressure along a single axial direction through a rigid plunger, or piston to achieve compacting. Pressing results in the direct contact of particles, reduces the average distance between particles, and changes the shape of particles. The apparent density of a compact is controlled by proper mixing of various particles size fractions.

To enhance the compacting, before pressing, the powder should be disaggregated by mixing the powder with solvent such as isopropanol in the ultrasonic bath or added a couple drops of acetone to reduce the surface tension.

Organic materials that provide a temporary bond between the ceramic particles are often required for pressing. These binders provide lubrication (free flowing) during pressing and give the pressed part enough strength and toughness that can be handled even machined prior to densification. The amount of binder required is quite low, typically ranging from 0.5 to 5%.

Binder selection is dependent on the type of pressing that will be conducted. Some binders such as waxes and gums are very soft and quite sensitive to temperature variations. These generally do not require moisture or lubricant additions prior to pressing, but must be handled more carefully to avoid changes in granule size that might alter flow characteristics into the pressing die or result in inhomogeneous density distribution. Other common binders such as polyvinyl alcohol and cellulose types, purchased, in a powder form, must be dissolved in water before admixing. Polyethylene glycol binder of a low molecular weight are relatively heat-stable viscous liquids. High-molecular-weight forms are waxy solids used as binders and lubricants.

2.4.4 Sintering [70, 71]

Sintering by definition is a process of permanent chemical and physical change accompanied by reduced porosity by the mechanism of grain growth and grain bonding. The driving force for sintering is the decrease in surface free energy that occurs as the surface area of the polycrystalline aggregate is reduced. This process can be achieved by solid state reaction or alternatively in the presence of a liquid phase.

When a powdered aggregate is sintered, necks form between the particles, and the aggregate may increase in density (Figure 2.4). The growth of the neck is due to the transport of matter or of the counter-flow of vacancies between the particles and the pores. In crystalline powder, its transport occurs by diffusion (bulk, surface, or grain boundary diffusion), whereas in amorphous materials, occurs by viscous flow. Kuczynski has defined the neck growth as in Equation (12)

$$X^n/r^m = kt \qquad (12)$$

Where X and r are defined in Figure 2.4, t is the time, k is the temperature dependent constant, n and m are constants dependent on the mechanisms of growth, viscous or bulk diffusion, surface diffusion, or evaporation and condensation.

Three stages of sintering can be distinguished.

1. The early stage or initial stages during which the necks form at points of particle contact and the particles center usually approach each other. At this stage the individual particles are still distinguishable.
2. The intermediate stage during which the necks become large, resulting in the formation of an interconnected pore structure.
3. The third, final stage during which the pores become isolated. Elimination of the interconnectivity of pores eliminates surface and vapor transport.

Closed pores isolated from grain boundaries shrink very slowly because grain boundary diffusion is far away from the pores. The growth of grains, therefore, hinders the attainment of theoretical density, since the pore's growth is also enhanced. It is essential, therefore, to retard grain growth so that densification of the compact can continue to the theoretical limit. This is particularly important with the present

trend of using ultrafine particles as starting materials for the fabrication of technical ceramics.

Surface diffusion becomes important in the case of very fine particles. Grain boundary diffusion and volume diffusion are the main mechanisms causing shrinkage of the neck, whereas surface diffusion does not contribute to any shrinkage. The most important diffusion paths during the sintering of two spheres with a grain boundary are surface diffusion, grain boundary diffusion, volume diffusion from the grain boundary to the neck surface, and volume diffusion from the sphere surface to the neck surface. The sintering rate is also affected by the crystallization and growth processes, which occur concurrently. The sintering rate is reduced when there is intensive grain growth because when diffusion form the pores occurs toward the boundaries of individual grains the distance over which diffusion occurs with a reduction in pores is determined by the size of the crystals.

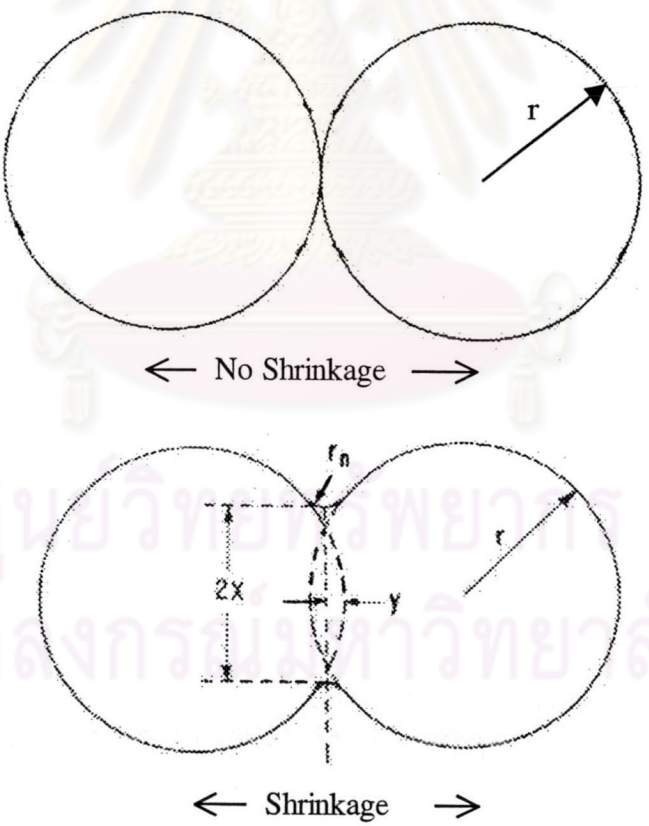

Figure 2.4 Mechanism of sintering; X is the internal radius of the neck, r is the particle radius, L is the shrinkage [72]

2.4.4.1 Sintering Temperature

It is convenient to define "sintering temperature", the temperature at which a given powder compact will densify to a certain desired density, about 90% of the theoretical density during a certain heating period. For the particles of the order of 1 μm in diameter, which are commonly used in ceramic work, a reasonable sintering temperature is approximately 0.75 of the absolute melting point.

One major difficulty lies in the inexact description of what is meant by "better" sintering. Normally, it means a higher-density product. Most scientific studies of sintering involve at least the measurement of the rate of shrinkage of specimens up to a shrinkage of several percent. In Equation (13), a shrinkage law of the type

$$\Delta L/L_0 = kt^n \qquad (13)$$

is commonly observed during the initial stage of sintering, where L_0 is the initial magnitude of some linear dimension of the powder compact, ΔL is the change in that dimension, and t is time. The exponent n range from 1/3 to ½ and k is inversely proportional to the cube of the particle radius.

If powder activity is measured by the initial sintering kinetics, it is universally observed that a fine powder sinters faster than a coarse one.

Itoh et al. [73] studied the sintering temperature of $La_{1-x}Sr_xCoO_3$ specimen when the temperature rose at a heating rate of 5 K/min. It was obvious that a 2-mm cube prepared by pressing the powder precursor transformed with increasing temperature, especially at > 1,200°C. The shrinkage rates, defined on the basis of 25°C reading of 1.0 along the width and height of the cubic specimen, with temperature were calculated and shown in Figure 2.5. Exceeding 1,200°C, a sudden shrinkage took place. Further, above 1,520°C, the specimen melted. Since it became evident that the specimen was significantly sintered in the range 1,000-1,257°C, the final sintering temperature was selected to be 1,250°C.

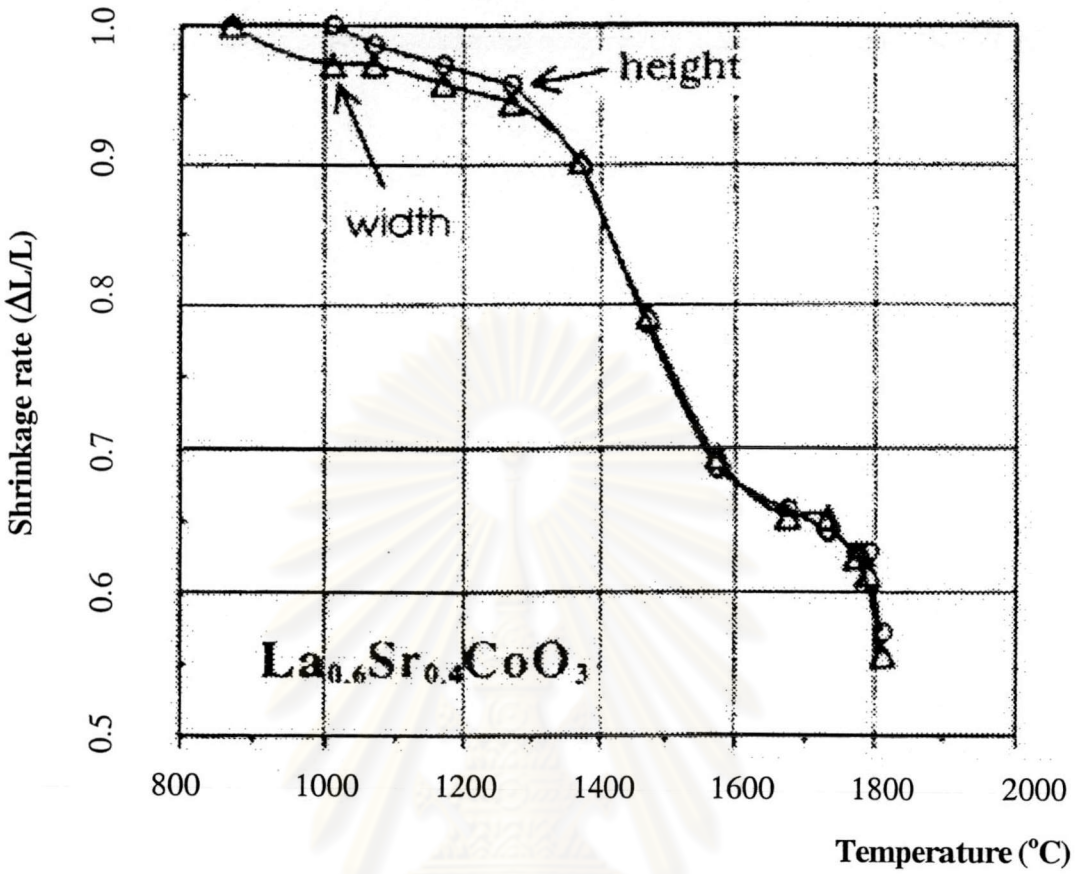

Figure 2.5 Shrinking rate versus temperature [43]

2.4.4.2 Other Reactions during Sintering [70]

Besides sintering, a number of other reactions also take place. These reactions can be grouped into the following categories:

2.4.4.2.1 Loss of Physical Water

Most green ceramics contain 1 to 3 % physical water when they are placed in a furnace. When the sintering process starts, this physical water comes off as water vapor between 100 and 200°C, which in essence completes the drying process.

2.4.4.2.2 Oxidation

Organic materials typically burn out between 300-400°C. Organic material is often added to green ceramic bodies as a temporary binder. The purpose of the temporary binder is to hold the green ceramic together so it can be handled and placed in a furnace. Another source of organic material in a green body is material such as saw dust, which is added to the body so it burns out to create porosity. Still another source of organic is naturally occurring organic in ball clay.

The carbon in these organics oxidizes to carbon dioxide ($C + O_2 \longrightarrow CO_2$) which is an exothermic reaction. In cases where a large amount of organic is present, it is sometimes necessary to go through the oxidation period with a relatively low oxygen level in a furnace. This slows down the oxidation process and prevents the ceramic from cracking due to excessive heat generated inside the piece by the CO_2 formation. In this case, a two-stage reaction occurs with formation of carbon monoxide ($2C + O_2 \rightarrow 2CO$) inside the piece which releases less heat than the carbon dioxide formation. Once the CO gas volatilizes out of the ceramic it then completes the oxidation to CO_2 in a furnace atmosphere and/or fuel which does not harm the ceramic.

It is important to oxidize all the carbon in a ceramic body and volatilize it out of the ceramic through the open pores before densification starts to close the pores. When this situation occurs, black coring will occur with pure carbon trapped inside the piece. Another possibility is bloating caused by CO or CO_2 trapped inside the piece by closed pores. To prevent black coring and bloating it may be necessary to slow down the sintering rate through the oxidation range.

The high percentage of organic and the large size of the ceramic piece will require the slow sintering rate. However, proper binder removal is normally accomplished by slowly raising the temperature to a level at which the binder volatilizes, and holding at this temperature until the binder is gone. The temperature can then be safely increased to the sintering temperature. However, if the temperature is increased before the binder has completely volatilized, the portion remaining will char and leave a residue of carbon.

2.4.4.2.3 Decomposition

The decomposition means "the loss of chemical molecule in the material" occurs between 400-1,450°C, depending on the materials. For example, the decomposition of Kaolin to Meta-Kaolin occurs by the reaction in Equation (14).

$$Al_2Si_2O_4(OH)_4 \longrightarrow Al_2Si_2O_6 + H_2O \qquad (14)$$

The decomposition of carbonates occurs between 400-1,000°C giving off CO_2.

2.4.4.2.4 Polymorphic Transformation [68]

As the temperature or the pressure on a material changes, inter-atomic distance and the level of atomic vibration changes such that the initial structure may not be the most stable structure under the new conditions. Materials having the same chemical composition but the different crystal structures are called polymorphs and the change from one structure to another is referred to as a polymorphic transformation.

Two types of polymorphic transformations occur. The first, displace transformation involves distortion of the structure, such as a change bond angle. The second type of transformation, the reconstructive transformation, involves breaking of bonds and formation of a new structure.

Polymorphism is common in ceramic materials and in many cases has a strong impact on the useful limits of the application of the material. For instance, the $La_{1-x}Sr_xMnO_3$ compound transforms from a rhombohedral to orthorhombic phase at the structure phase transition temperature with decreasing temperature. When the rhormbohedral phase transforms into an orthorhombic phase, the Mn-O-Mn bond angle becomes smaller [73]. Some perovskite-type materials may go through the polymorphic transformation during sintering or later oxygen-permeation measurements.

Polymorphic transformations do not usually cause problems during sintering, but can cause problems during cool-down after sintering if a sudden volume change is involved. No problem occurs during heat-up because the individual particles are not constrained. However, after sintering, the original particles are now grains, which are solidly bonded to each other and thus restrained. When the component goes through

the transformation temperature, the grains are not free to move. Very high internal stress results at the grain boundaries and many cracks are initiated, significantly weakening the material. Therefore, the rate of heating or cooling reactors has to be carefully controlled.

2.4.4.2 The Effect of Processing Conditions on Sintering Procedure [74]

Generally it is not easy to obtain a pore-free disk from a ceramic powder as the starting material. Some ideas have been proposed to carry out the sintering process successfully: (1) to apply an extremely high temperature; (2) to control the distribution of particle diameter; (3) to use an additive such as polyvinyl alcohol; (4) to utilize a chemical reaction and (5) to employ HIP (hot isotropic pressing), or molten particle deposition. Besides these techniques, the processing conditions affect the density of the membrane.

First, it was absolutely necessary to protect the pre-calcined materials from their interaction with the surrounded air before sintering. After 10-20 hours of their storage in air at room temperature considerable increase in the volume of not sintered samples was seen even visually. As mentions above, the other reactions during sintering are composed of loss of physical water, oxidation, decomposition, and phase transformation. These reactions cause the formation of pores due to entrapment of gases released form the sample. The extent of porosity could not be significantly decreased by means of only higher temperatures or longer periods of sintering. But the porosity was strongly determined by the rate of heating at different sections of the whole reaction during sintering of membrane. Therefore, the heating ramp should be stopped at 100-200°C for evporating the water, and 400-500°C for oxidation organic materials, and then raised to sintering temperature.

The pre-calcination temperature also affects the sinterability. Gorelove et al. [75] revealed that the density of the samples decreased with increasing pre-calcination temperature of the initial mixture. $La_{0.8}Sr_{0.2}Ga_{0.85}Mg_{0.15}O_{3-\delta}$, pre-calcined at 1,100 and 1,400°C and sintered at 1,300°C for 1 hour had the relative density of 81% and 70% of the theoretical value, respectively. Even when the sintering lasted at 1,420°C for 15 hours, the samples still had considerably different density values 95% and 89%, respectively. The loss of sinterability when increasing the calcination

temperature of starting materials is well known among the ceramists. The effect of the pre-calcination temperature on the ceramic density decreased progressively as the sintering temperature was raised, and diminished almost completely at the sintering temperature of 1,520°C. When the samples were sintered at 1,520°C for 10 hours, their density values became 98% and 97%, respectively.

2.4.4.3 The Effect of Material Compositions on Sintering Property

Kleveland et al. [75] prepared $La_{1-x}M_xCoO_{3-\delta}$ (M = Ca, Sr; x = 0.2) powders by using the glycin-nitrate and the EDTA methods. They reported that the substitution of La with Sr or Ca in $LaCoO_3$ decreased the sintering temperature in the order $LaCoO_3$ > 20% Sr > 20%Ca. Besides, the control of the stoichiometry of $LaCoO_3$ based ceramics is important in order to obtain dense materials with well defined microstructure. The presence of other crystalline phases in addition to the perovskite due to Co-excess-/-deficiency considerably affects the microstructure and acts as grain growth inhibitors by grain boundary pinning. The volume fraction of secondary phases is particularly large in the case of Co-deficient $LaCoO_3$ due to the formation of La_2O_3 and $La_4Co_3O_{10}$. Because of the lower low crystallographic density of these secondary phases, the theoretical density of the Co-deficient material is lower than this stoichiometric sample. At Co-excess a higher porosity is observed. The product from the decomposition of Co_3O_4 during sintering above 900°C, CoO, inhibits sintering of the material. The melting point for CoO is considerably higher than that for $LaCoO_3$, and the sintering temperature will be higher for the two-phase mixture than that for single phase $LaCoO_3$.

In non-stoichiometric $La_{0.8}Ca_{0.2}CoO_3$, a liquid phase consisting mainly of CaO and CoO was observed at 1,400°C causing exaggerated grain growth. Considerable pore coarsening was observed in Co-excess $La_{0.8}Ca_{0.2}CoO_3$ at 1,350°C.

Lanthanum chromite perovskites, with stoichiometric composition, are known to be chemically stable under oxidizing or reducing atmospheres at high temperatures, as well as being poorly sinterable in air. The reason for the poor sintering is that the chromium-vapor component starts to evaporate as gaseous CrO_3 from the $LaCrO_3$ particles at temperatures over 1,000°C. This incongruent vaporization heterogenization mechanism disturbs the densification of the $LaCrO_3$ particles by evaporation, which reduces the ability to produce a dense sintered body [76].

Mori et al. [76] studied the sintering behavior of La_xCrO_3 with non-stoichiometry of A site. The XRD patterns indicated that the La_xCrO_3 with $x > 1.0$ showed two phases with orthorhombic and rhombohedral symmetry of $LaCrO_3$ perovskite and La_2O_3, and those with $x < 1.0$ showed two phases of $LaCrO_3$ and Cr_2O_3. The relatively densities increased remarkably with excess La_2O_3. Since no liquid phase appeared and no reaction occurred during the sintering process, chromium vapor was suppressed by excess in the lanthanum chromites, and the densification proceeded. However, the La_xCrO_3 samples with $x \geq 1.02$ were not stable in air, because La_2O_3 in the samples reacted with moisture and formed $La(OH)_3$. Because the formation of $La(OH)_3$ causes a volume change, the samples broke down.

Mori et al. [77] further studied the sintering behavior of Ca- or Sr-doped $LaCrO_3$ perovskites, $La_{1-x}AE_xCrO_3$ (AE = Ca and Sr), $0 \leq x \leq 0.3$. The relative density of both perovskites, after firing at 1,600°C for 20 hours, increased with increasing AE content. When $x \leq 0.2$, the sintering properties of $La_{1-x}Ca_xCrO_3$ were lower than $La_{1-x}Sr_xCrO_3$. However the reverse results were observed at $x = 0.3$.

Stevenson et al. [78] showed the Ga_2O loss from lanthanum gallate samples could occur in the temperature range used in sintering and might account for the observed bloating of some specimens. $LaGaO_3$ doped with Sr and Mg (LSGM) was synthesized using a combustion synthesis technique. The synthesized powders were sintered to high density in air, although excessively high sintering temperatures in the 1,400 to 1,600°C led to bloating of samples, possibly due to the volatilization of Ga_2O from the perovskite structure. When sintered at temperatures greater than 1,600°C, bloating might be related to the tendency for gallium (III) oxide to be reduced to gallium(I) oxide, following in Equation (15);

$$Ga_2O_3\,(s) \leftrightarrow Ga_2O\,(g) + O_2\,(g) \qquad (15)$$

Since a net loss of specimen mass and an increase in specimen volume due to bloating, the decrease in sintered density was observed at the high temperature, especially in Ga enriched compositions ($x = 0.90$-0.95).

Ahmad-Khanlou et al. [79] investigated the crystalline phases, sintering behavior, and microstructure of the compound $La_{0.8}Sr_{0.2}Ga_{0.9+x}Mg_{0.1}O_{3-\delta}$

($-0.02 < x < 0.04$) as a function of the Ga content. Depending on thermal treatment and Ga content, the compound $LaSrGa_3O_7$, $SrLaGaO_4$, and La_2O_3 were identified in addition to the perovskite phase. With increasing sintering temperature, the XRD examinations showed that $SrLaGaO_4$ was present at 1,300°C, whereas its content was significantly decreased at 1,400°C. Since this compound had a melting point at approximately 1,400°C , decomposition and Ga_2O evaporation might be expected. The expectation was confirmed by the observation of the increase of volume with increasing of temperature, 1,400-1,500°C. The fractions of lanthanum gallate and $LaSrGaO_4$ decreased in favor of $LaSrGa_3O_7$ with increasing Ga content and with increasing temperature. The tendency of Ga evaporation should therefore also decrease with decreasing $LaSrGaO_4$ content.

There are several factors affecting the Ga vaporization from the doped $LaGaO_3$ such as the temperature, the oxygen partial pressure, and the composition of dopant. Since the Ga vaporization have not yet been widely reported, it should be further studied.